In vivo interrogation of gene function in the mammalian brain using CRISPR-Cas9

Lukasz Swiech[1–3,6], Matthias Heidenreich[1–3,6], Abhishek Banerjee[4], Naomi Habib[1–3], Yinqing Li[1,2,5], John Trombetta[1], Mriganka Sur[4] & Feng Zhang[1–3]

Probing gene function in the mammalian brain can be greatly assisted with methods to manipulate the genome of neurons *in vivo*. The clustered, regularly interspaced, short palindromic repeats (CRISPR)-associated endonuclease (Cas)9 from *Streptococcus pyogenes* (SpCas9)[1] can be used to edit single or multiple genes in replicating eukaryotic cells, resulting in frame-shifting insertion/deletion (indel) mutations and subsequent protein depletion. Here, we delivered SpCas9 and guide RNAs using adeno-associated viral (AAV) vectors to target single (*Mecp2*) as well as multiple genes (*Dnmt1*, *Dnmt3a* and *Dnmt3b*) in the adult mouse brain *in vivo*. We characterized the effects of genome modifications in postmitotic neurons using biochemical, genetic, electrophysiological and behavioral readouts. Our results demonstrate that AAV-mediated SpCas9 genome editing can enable reverse genetic studies of gene function in the brain.

The SpCas9 nuclease can be reprogrammed to target specific genomic loci in mammalian cells using single guide RNAs (sgRNAs) and has been used in a variety of genome editing applications[1]. Recently, SpCas9 has been applied in mice using hydrodynamic injection[2,3] and adenovirus delivery[4] in the liver. To enable SpCas9 use for editing cells in the mammalian nervous system *in vivo*, we sought to adapt a set of AAV vectors that are commonly used for brain gene delivery. Because of the packaging size limitation of AAV vectors[5], we designed a dual-vector system that packages SpCas9 (AAV-SpCas9) and sgRNA expression cassettes (AAV-SpGuide) in two separate viral vectors (**Fig. 1a**).

We assessed various, short, neuron-specific promoters as well as polyadenylation signals to achieve efficient packaging of SpCas9 in AAV vectors. For our final design we chose a truncated version of the mouse *Mecp2* promoter (235 bp, pMecp2) and a minimal polyadenylation signal (48 bp, spA)[6]. To identify SpCas9-expressing neurons, we tagged SpCas9 with an HA-epitope tag (**Supplementary Fig. 1**). For the AAV-SpGuide vector, we packaged a U6-sgRNA expression cassette together with the green fluorescent protein (GFP) fused to the KASH nuclear transmembrane domain[7] driven by the human Synapsin I promoter (**Fig. 1a**). The KASH domain directs the fused GFP protein

to the outer nuclear membrane and enables identification of neurons transduced by AAV-SpGuide (**Supplementary Fig. 2a,b**).

To test the delivery efficacy of our dual-vector system, we first transduced primary mouse cortical neurons *in vitro*. We observed robust expression of AAV-SpCas9 and AAV-SpGuide, with a co-transduction efficiency of ~75% (**Supplementary Fig. 2b,c**). AAV-mediated expression of SpCas9 did not adversely affect the morphology and survival of transduced neurons (**Supplementary Figs. 1c** and **2b,d**).

We next sought to test SpCas9-mediated genome editing in mouse primary neurons. First we targeted an X-chromosomal gene, *Mecp2* (methyl CpG binding protein), which plays an important role in the pathogenesis of Rett syndrome[8]. MeCP2 is ubiquitously expressed in neurons throughout the brain, and its deficiency has been shown to be associated with severe morphological and electrophysiological phenotypes in neurons as well as misregulation of gene expression, all of which are thought to contribute to the neurological symptoms of Rett syndrome[9–11]. We designed several sgRNAs targeting exon 3 of the mouse *Mecp2* gene and evaluated their effectiveness in indel generation in the Neuro-2a cells. The most efficient sgRNA (*Mecp2* target 5, **Supplementary Fig. 3**) was used in subsequent *in vitro* and *in vivo Mecp2* targeting experiments.

To assess the editing efficiency of our dual-vector system, we transduced mouse primary cortical neurons with SpCas9 and *Mecp2*-targeting sgRNA or control sgRNA (targeting the bacterial *lacZ* gene). Using immunocytochemistry we observed that >70% of cells transduced with *Mecp2*-targeting sgRNA were MeCP2-negative 7 d post-transduction (**Supplementary Fig. 4a,b**). We also confirmed a corresponding decrease in MeCP2 protein levels using western blot analysis (**Supplementary Fig. 4c**). Binding by the catalytically inactive SpCas9 (D10A/H840A, dSpCas9) may repress gene expression by blocking transcription[12–14]. To test that possibility, we co-expressed dSpCas9 and *Mecp2*-targeting sgRNA in neurons. We did not observe any reduction in protein levels (**Supplementary Fig. 4a–c**), suggesting that MeCP2 knockdown is likely due to indels in the *Mecp2* locus (**Supplementary Fig. 4d**). To assess efficiency of *Mecp2* modification in targeted cells, we purified GFP-KASH+ nuclei using fluorescence-activated cell sorting (FACS) (**Supplementary Fig. 4e,f**) and sequenced

[1]Broad Institute of MIT and Harvard, Cambridge, Massachusetts, USA. [2]McGovern Institute for Brain Research, Department of Brain and Cognitive Sciences, Massachusetts Institute of Technology, Cambridge, Massachusetts, USA. [3]McGovern Institute for Brain Research, Department of Biological Engineering, Massachusetts Institute of Technology, Cambridge, Massachusetts, USA. [4]Picower Institute for Learning and Memory, Department of Brain and Cognitive Sciences, Massachusetts Institute of Technology, Cambridge, Massachusetts, USA. [5]Department of Electrical Engineering and Computer Science, Massachusetts Institute of Technology, Cambridge, Massachusetts, USA. [6]These authors contributed equally to this work. Correspondence should be addressed to F.Z. (zhang@broadinstitute.org).
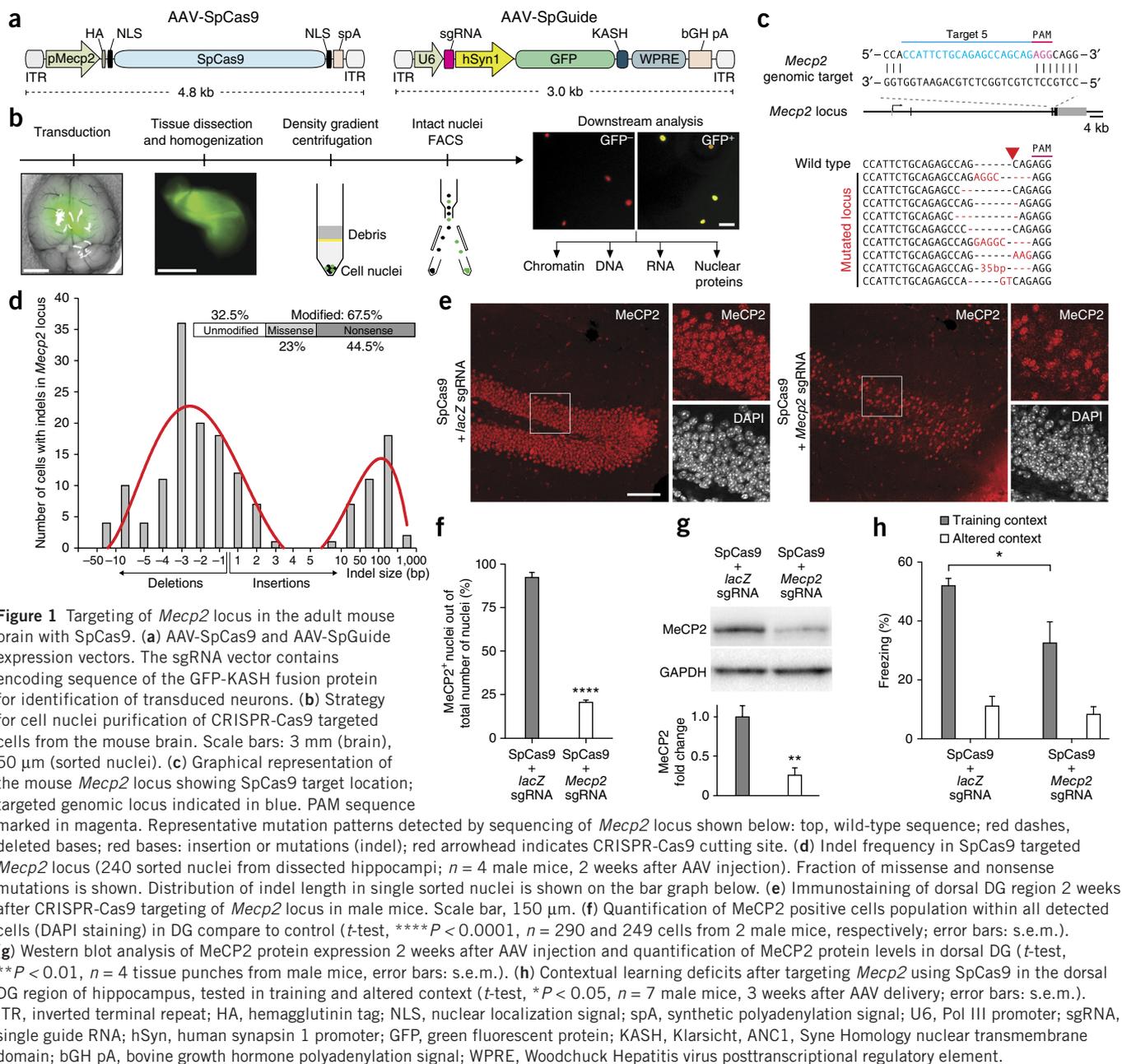
Figure 1 Targeting of *Mecp2* locus in the adult mouse brain with SpCas9. (**a**) AAV-SpCas9 and AAV-SpGuide expression vectors. The sgRNA vector contains encoding sequence of the GFP-KASH fusion protein for identification of transduced neurons. (**b**) Strategy for cell nuclei purification of CRISPR-Cas9 targeted cells from the mouse brain. Scale bars: 3 mm (brain), 50 μm (sorted nuclei). (**c**) Graphical representation of the mouse *Mecp2* locus showing SpCas9 target location; targeted genomic locus indicated in blue. PAM sequence marked in magenta. Representative mutation patterns detected by sequencing of *Mecp2* locus shown below: top, wild-type sequence; red dashes, deleted bases; red bases: insertion or mutations (indel); red arrowhead indicates CRISPR-Cas9 cutting site. (**d**) Indel frequency in SpCas9 targeted *Mecp2* locus (240 sorted nuclei from dissected hippocampi; *n* = 4 male mice, 2 weeks after AAV injection). Fraction of missense and nonsense mutations is shown. Distribution of indel length in single sorted nuclei is shown on the bar graph below. (**e**) Immunostaining of dorsal DG region 2 weeks after CRISPR-Cas9 targeting of *Mecp2* locus in male mice. Scale bar, 150 μm. (**f**) Quantification of MeCP2 positive cells population within all detected cells (DAPI staining) in DG compare to control (*t*-test, ****$P < 0.0001$, *n* = 290 and 249 cells from 2 male mice, respectively; error bars: s.e.m.). (**g**) Western blot analysis of MeCP2 protein expression 2 weeks after AAV injection and quantification of MeCP2 protein levels in dorsal DG (*t*-test, **$P < 0.01$, *n* = 4 tissue punches from male mice, error bars: s.e.m.). (**h**) Contextual learning deficits after targeting *Mecp2* using SpCas9 in the dorsal DG region of hippocampus, tested in training and altered context (*t*-test, *$P < 0.05$, *n* = 7 male mice, 3 weeks after AAV delivery; error bars: s.e.m.). ITR, inverted terminal repeat; HA, hemagglutinin tag; NLS, nuclear localization signal; spA, synthetic polyadenylation signal; U6, Pol III promoter; sgRNA, single guide RNA; hSyn, human synapsin 1 promoter; GFP, green fluorescent protein; KASH, Klarsicht, ANC1, Syne Homology nuclear transmembrane domain; bGH pA, bovine growth hormone polyadenylation signal; WPRE, Woodchuck Hepatitis virus posttranscriptional regulatory element.

the *Mecp2* locus using targeted next-generation sequencing (NGS). We found that ~65% of the GFP-KASH⁺ nuclei (*n* = 103) were genetically modified within the *Mecp2* locus. MeCP2 loss-of-function can lead to dendritic tree abnormalities and spine morphogenesis defects in neurons[10,11]. Therefore, we investigated whether SpCas9-mediated MeCP2 depletion in cultured neurons could recapitulate these morphological phenotypes. Neurons co-expressing SpCas9 and *Mecp2*-targeting sgRNA exhibited altered dendritic tree morphology and spine density when compared with control neurons (*lacZ*-targeting sgRNA) (**Supplementary Fig. 5**).

Efficient editing of neuronal genes *in vivo* would enable direct testing of gene function in relevant cell types embedded in their native contexts. Therefore, we tested whether CRISPR-Cas9 could mediate stable genomic modifications in neurons in the brains of living mice. We stereotactically injected a mixture (1:1 ratio) of AAV-SpCas9 and AAV-SpGuide (*Mecp2*- or *lacZ*-targeting sgRNAs) into the hippocampal

dentate gyrus (DG) of adult male mice. We observed ~80% co-transduction efficiency of both vectors (GFP-KASH⁺/HA-Cas9⁺ cells by means of co-staining) in hippocampal granule cells at 4 weeks after viral injection (**Supplementary Fig. 6**).

Isolation of subsets of cells from heterogeneous brain tissue for downstream analysis can be achieved by fluorescent labeling of cells followed by FACS. However, due to the complex morphology of neurons, dissociation of individual cells from adult brain tissue is a major impediment to subsequent analyses[15]. Therefore, we established a protocol to purify intact nuclei of transduced cells from dissected brain tissue (**Fig. 1b**). Using NGS, we quantified indel formation in the targeted *Mecp2* locus at the single-cell level and found that ~68% of targeted cells contained indel mutations 2 weeks after viral delivery (**Fig. 1c,d**). The number of MeCP2-positive nuclei in the DG was decreased by ~70% in the DG of animals injected with AAV-SpCas9 and *Mecp2*-targeting sgRNA. Total MeCP2 protein levels were also decreased by >60% (**Fig. 1e–g**). These

Figure 2 Analysis of gene expression in SpCas9-mediated MeCP2 knockdown neurons. Hierarchical clustering of differentially expressed genes (*t*-test, 0.01 FDR, *n* = 19 populations of sorted nuclei from 8 male mice, 2 weeks after AAV delivery) detected by RNA-seq. Relative log(TPM+1) expression levels of genes are normalized for each row and displayed in red-blue color scale. Each column represents a population of targeted 100 neuronal nuclei FACS sorted from the isolated, dentate gyrus population of cells, either from *Mecp2* or control (*lacZ*) sgRNA transduced animals, as indicated. TPM, transcripts per million.

results demonstrate the efficiency of AAV-mediated genome editing in the adult brain and suggest that SpCas9 can be used to directly perturb specific genes within intact biological contexts.

MeCP2 has a fundamental role in learning, which can be measured by the contextual fear-conditioning paradigm (CFC)[16]. The dorsal DG region is the structure crucial for contextual learning[17]. Given the efficient depletion of MeCP2 in the DG we investigated the behavioral consequences of *Mecp2* gene editing. CFC behavioral tests revealed that CRISPR-Cas9–mediated inactivation of MeCP2 in the DG impaired contextual memory (**Fig. 1h**), similar to what was previously observed in MeCP2 mutant mice[16]. No difference was observed when mice were tested in an altered context, suggesting contextual specificity of the memory trace. In contrast, *Mecp2* knockdown mice did not exhibit any altered behavior in open field testing, novel object recognition or the elevated plus maze. These data suggest that the MeCP2 depletion in the dorsal DG affects contextual learning but leaves other cognitive abilities intact (**Supplementary Fig. 7**).

In vivo genome editing in neurons may also be used to study cellular processes, such as transcription dynamics. Depletion of MeCP2 is known to result in genome-wide transcriptional dysregulation[18], which may contribute to learning deficits. To test the effect of MeCP2 knockdown on the transcription state of adult neurons in the DG, we sequenced mRNA from FACS-purified GFP-KASH+ nuclei from dissected DG tissue (**Fig. 1b** and **Supplementary Fig. 8**). Out of 556 highly expressed genes, we found 34 differentially expressed between neurons receiving *Mecp2*- and *lacZ*-targeting sgRNAs (**Fig. 2** and **Supplementary Fig. 9**). These results show that the combination of SpCas9-mediated genome perturbation, intact nuclei purification and RNA-seq analysis provides a robust method to study transcriptional regulation in adult neurons *in vivo* and identify candidate genes that might modulate specific neuronal functions or disease processes.

We next analyzed the effect of genomic perturbation of *Mecp2* on the physiological properties of targeted cells in intact brain circuits. Primary visual cortex (V1) has long been a model for deciphering mechanisms underlying integrative responses of cortical neurons, including orientation selectivity, a crucial response feature created within V1 (ref. 19). The effects of MeCP2 on cortical circuits that create such responses are unresolved[20]. We stereotactically injected AAV-SpCas9 and AAV-SpGuide targeting *Mecp2* into the superficial layers of V1 (**Fig. 3a**). Two weeks later, we performed *in vivo* two-photon-guided cell-attached recordings in anesthetized mice (**Fig. 3b,c**) to compare the electrophysiological responses of excitatory GFP-KASH+ neurons with neighboring control neurons expressing GFP-KASH and *lacZ* gRNA, respectively. V1 neurons are selectively tuned to respond to a specific orientation of a visual stimulus, a parameter that can be measured as orientation selectivity index (OSI). Responses to a full range of oriented drifting gratings (**Fig. 3d,e**) showed that the OSI was reduced in GFP-KASH+ neurons targeted with *Mecp2* sgRNA (**Fig. 3f**), along with peak responses at the optimal orientation (**Fig. 3g**) when compared to *lacZ* sgRNA expressing-control neurons. Previous studies have reported decreased synaptic drive to pyramidal neurons in hippocampal slices of germline *Mecp2*
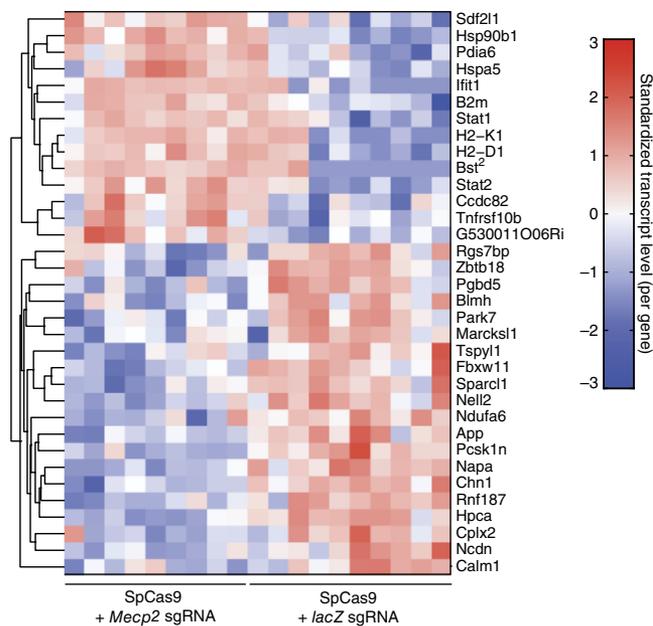
knockout mice[21] and after short hairpin RNA-mediated knockdown of MeCP2 in mouse motor cortex[22]. These experiments confirm that alterations in visual drive and tuning occur in genome-edited neurons in functional circuits. Cas9-mediated MeCP2 depletion in adult mice underscores the maintenance role of MeCP2 in adult brain[23] and reveals the role of MeCP2 in the integration of inputs that underlie a cortical response feature; it further demonstrates the versatility of SpCas9 in facilitating targeted gene knockdown in the mammalian brain *in vivo* for studying gene function in health and disease.

Many cellular processes affecting physiological and neuropathological conditions are controlled by groups of genes, some of which have compensatory roles. Therefore, targeting only one gene in a network may not provide sufficient perturbation for the biological process of interest. To test whether SpCas9 could be used for multiplex genome editing in the brain, we designed an expression vector with three U6-sgRNA cassettes in tandem, along with GFP-KASH for nuclei labeling (**Fig. 4a**). We chose sgRNAs targeting the family of DNA methyltransferases (DNMTs: *Dnmt1*, *Dnmt3a* and *Dnmt3b*). *Dnmt1* and *Dnmt3a* are highly expressed in the adult brain and are required for synaptic plasticity, learning and memory formation[24]. As *Dnmt1* and *Dnmt3a* were shown to be mutually redundant in these cognitive processes[24], they are good targets for testing multiplex gene editing. To avoid any potential compensatory effects by *Dnmt3b*, we also targeted this gene even though it is mainly expressed during neurodevelopment[24]. We selected individual sgRNAs for simultaneous targeting of DNMTs genes by testing their efficiencies using the Neuro-2a cell line (**Fig. 4b** and **Supplementary Fig. 10**).

To test the efficacy of multiplex genome editing *in vivo*, we stereotactically injected a mixture of AAV-SpCas9 and AAV-SpGuide (targeting *Dnmt3a*, *Dnmt1* and *Dnmt3b*) into the DG of adult mice. After 8 weeks, individual nuclei from transduced cells were analyzed with NGS. We detected indels in all three loci with ~75% modification rate in *Dnmt1* and *Dnmt3a*, and ~50% in *Dnmt3b* (**Fig. 4c** and **Supplementary Fig. 11**).

Recent studies with SpCas9 have shown that when genomic loci partially match the sgRNA, the result can be off-target indel formation[25,26]. We computationally identified highly similar genomic target sites[26] and quantified the rate of modifications using NGS. Indel analysis of the top predicted off-target loci in sorted nuclei from transduced
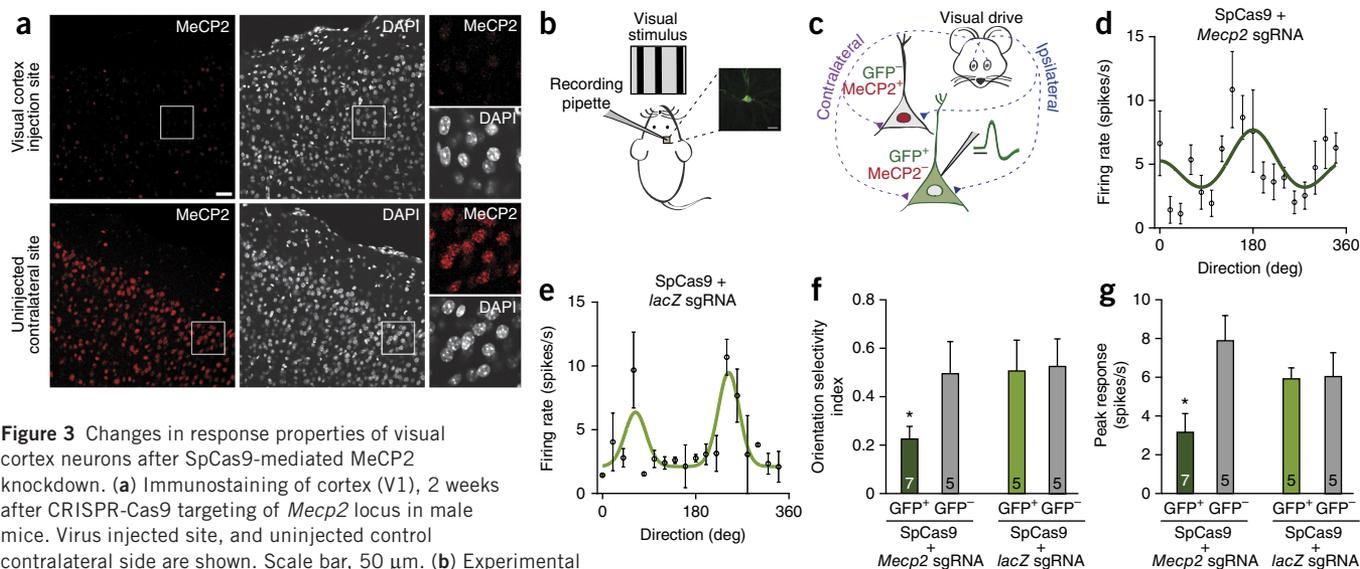
Figure 3 Changes in response properties of visual cortex neurons after SpCas9-mediated MeCP2 knockdown. (**a**) Immunostaining of cortex (V1), 2 weeks after CRISPR-Cas9 targeting of *Mecp2* locus in male mice. Virus injected site, and uninjected control contralateral side are shown. Scale bar, 50 µm. (**b**) Experimental configuration. To assess visual responses of neurons in primary visual cortex (V1), we presented visual stimuli (oriented gratings) on an LCD monitor placed in front of anesthetized mice. Two weeks before experiment, mixture of SpCas9 with either *Mecp2* sgRNA or control sgRNA (*lacZ*) was stereotactically injected in V1. GFP-KASH+ neurons and GFP-KASH− neurons were recorded. Example of recorded GFP-KASH+ neuron is shown. Scale bar, 20 µm. (**c**) *In vivo* targeted cell-attached recording configuration from V1 layer 2/3 excitatory neurons that receive visual drive (ipsilateral and contralateral input). Genome modified GFP-KASH+/MeCP2− cells are shown in green, unmodified GFP-KASH−/MeCP2+ cells in gray. Recording pipette is indicated. Normalized mean spike shape (green) shows regular spiking excitatory neurons. Scale bar, 1 ms. (**d,e**) Orientation-selective responses of typical GFP-KASH+ neurons expressing *Mecp2* sgRNA (**d**) or *lacZ* sgRNA (**e**). (**f,g**) Orientation selectivity index (**f**) and peak responses (**g**) (spikes/s) measured from GFP-KASH+ cells expressing *Mecp2* and control sgRNA, respectively, and comparison with GFP-KASH− cells (*$P < 0.05$, t-test; numbers on bars indicate numbers of recorded cells; $n = 2$–3 animals per group; error bars: s.e.m.).

brain tissue (AAV-SpCas9 and AAV-SpGuide targeting *Dnmt1*, *Dnmt3a* and *Dnmt3b*) revealed a 0–1.6% indel formation, suggesting that SpCas9 did not cause pervasive off-target mutagenesis in these animals (**Supplementary Table 1**).

Although previous *in vivo* studies using SpCas9 analyzed population-averaged indel frequency[2,3], two important questions remain open, namely, how efficiently are both alleles of targeted genes modified, and what is the effectiveness of simultaneous targeting of multiple

loci in single cells? We first examined, using targeted sequencing of single nuclei, the frequency of cells in which both alleles of *Dnmt* were disrupted. Our results show biallelic modification of *Dnmt1* in >60% of transduced cells, and 42% and 17% of transduced cells for *Dnmt3a* and *Dnmt3b*, respectively (**Fig. 4c**). Observed differences in indel formation between different loci may be due to variations in the chromatin state and accessibility of target sites. Next, we quantified multiplex targeting efficiency at each *Dnmt* locus (**Fig. 4d**).

Figure 4 Simultaneous, multiplex gene editing in the mouse brain. (**a**) Schematic illustration of AAV vectors for multiplex genome targeting. (**b**) Graphical representation of targeted DNMT mouse loci. Targeted genomic loci are indicated in blue. PAM sequences are marked in magenta. (**c**) Next-generation sequencing-based analysis of indel frequency formation within *Dnmt1*, *Dnmt3a* and *Dnmt3b* loci analyzed in single neuronal nuclei. Fractions of mono- and biallelic modification are shown ($n = 79$ cells). (**d**) NGS analysis of *DNMTs* loci modification in single cells, showing co-occurrence of modification in multiple loci. (**e**) Western blot analysis for Dnmt3a and Dnmt1 proteins after *in vivo* delivery of CRISPR-Cas9 system targeting DNMT family genes in neurons (top). Western blot quantification of Dnmt3a and Dnmt1 protein levels in DG after *in vivo* CRISPR-Cas9 targeting (bottom; t-test, **$P < 0.001$, *$P < 0.05$, Dnmt3a: $n = 7$; Dnmt1: $n = 5$ from 5 animals; error bars: s.e.m.). (**f**) Contextual learning deficits, 8 weeks after targeting of DNMT genes using SpCas9 in the DG region of hippocampus, tested in training and altered context (t-test, ***$P < 0.001$, $n = 18$ animals; error bars: s.e.m.).
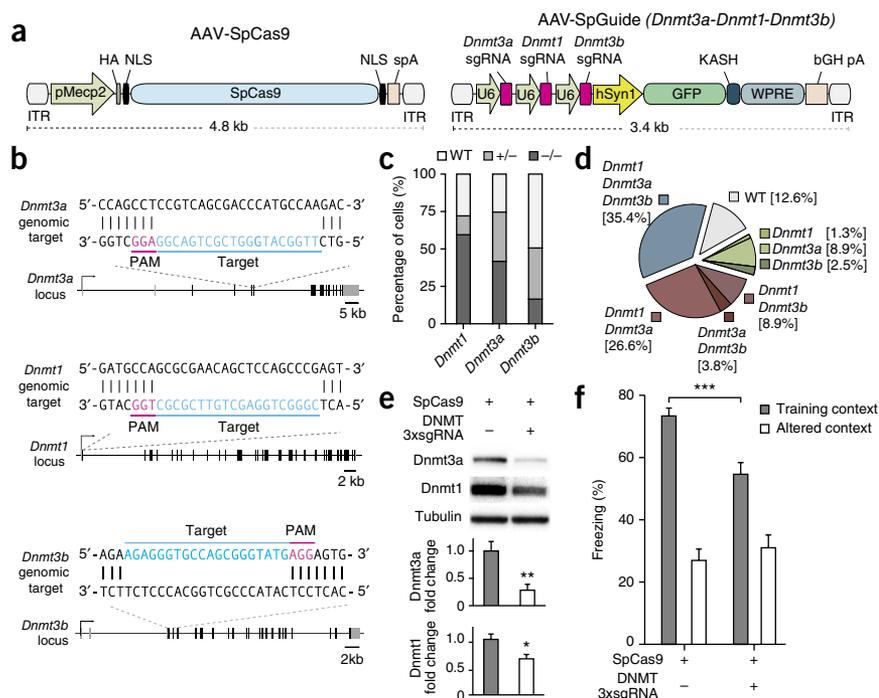
Approximately 62% of all transduced neurons contained indels in both *Dnmt1* and *Dnmt3a*, whereas simultaneous modification of *Dnmt1*, *Dnmt3a* and *Dnmt3b* was found in ~35% of all transduced neurons. These results are consistent with Dnmt3a and Dnmt1 protein depletion levels in the DG (**Fig. 4e**). Because of the low expression levels of *Dnmt3b* in the adult brain, we were not able to detect Dnmt3b protein using western blot analysis.

Dnmt3a and *Dnmt1* knockout mice have previously been reported to show altered hippocampal-dependent memory formation[24]. Owing to potentially compensatory functions, both genes need to be depleted for learning deficits to be observed. We therefore performed CFC behavior tests to investigate the effect of SpCas9-mediated knockdown of DNMTs on memory acquisition and consolidation. Triple DNMT knockdown mice showed impaired memory formation when tested under trained context conditions (**Fig. 4f**). However, no phenotype was observed in the open field, elevated plus maze and novel object recognition tests (**Supplementary Fig. 12**). In contrast to classical mouse models, which feature complete gene knockout, AAV-SpCas9 mediated knockdown may only provide perturbation in a fraction of targeted cells. Therefore, applications of the current AAV-SpCas9 system in complex tissues should be carefully designed and may be most effective for studying the effect of loss-of-function mutations on cell-autonomous properties.

AAV-mediated *in vivo* delivery of SpCas9 and sgRNA provides a rapid and powerful technology for precise genomic perturbations *in vivo*. We show that SpCas9 can be used to edit the genome of post-mitotic neurons in adult mice with high efficiency. SpCas9-mediated genomic perturbations can be readily combined with biochemical, sequencing, electrophysiological and behavioral analyses to study the function of the targeted genomic elements. SpCas9-mediated targeting of single or multiple genes can induce phenotypes similar to those previously observed in classic genetic mouse models. The use of SpCas9 not only necessitates the use of two AAV vectors, but also limits the size of promoter elements that can be used to achieve cell type–specific targeting. Given the diversity of Cas9 orthologs, some of which are substantially shorter than SpCas9 (refs. 27–29), it may be possible to engineer single AAV vectors that express both Cas9 and sgRNA, or Cas9 can be integrated to the genome to reduce the delivery burden[30]. Cas9 may also be combined with Cre-Lox systems to restrict Cas9-mediated genome editing to specific neuronal subtypes or circuit elements, thereby enhancing the ability of the CRISPR-Cas9 technology to dissect gene functions in brain processes.

METHODS

Methods and any associated references are available in the online version of the paper.

SRA accession code: PRJNA262918.

Note: Any Supplementary Information and Source Data files are available in the online version of the paper.

COMPETING FINANCIAL INTERESTS
The authors declare competing financial interests: details are available in the online version of the paper.

Reprints and permissions information is available online at http://www.nature.com/reprints/index.html.

1. Hsu, P.D., Lander, E.S. & Zhang, F. Development and applications of CRISPR-Cas9 for genome engineering. *Cell* **157**, 1262–1278 (2014).
2. Xue, W. *et al.* CRISPR-mediated direct mutation of cancer genes in the mouse liver. *Nature* doi:10.1038/nature13589 (6 August 2014).
3. Yin, H. *et al.* Genome editing with Cas9 in adult mice corrects a disease mutation and phenotype. *Nat. Biotechnol.* **32**, 551–553 (2014).
4. Ding, Q. *et al.* Permanent alteration of PCSK9 with *in vivo* CRISPR-Cas9 genome editing. *Circ. Res.* **115**, 488–492 (2014).
5. Wu, Z., Yang, H. & Colosi, P. Effect of genome size on AAV vector packaging. *Mol. Ther.* **18**, 80–86 (2010).
6. Gray, S.J. *et al.* Optimizing promoters for recombinant adeno-associated virus-mediated gene expression in the peripheral and central nervous system using self-complementary vectors. *Hum. Gene Ther.* **22**, 1143–1153 (2011).
7. Ostlund, C. *et al.* Dynamics and molecular interactions of linker of nucleoskeleton and cytoskeleton (LINC) complex proteins. *J. Cell Sci.* **122**, 4099–4108 (2009).
8. Chahrour, M. & Zoghbi, H.Y. The story of Rett syndrome: from clinic to neurobiology. *Neuron* **56**, 422–437 (2007).
9. Chen, R.Z., Akbarian, S., Tudor, M. & Jaenisch, R. Deficiency of methyl-CpG binding protein-2 in CNS neurons results in a Rett-like phenotype in mice. *Nat. Genet.* **27**, 327–331 (2001).
10. Li, Y. *et al.* Global transcriptional and translational repression in human-embryonic-stem-cell-derived Rett syndrome neurons. *Cell Stem Cell* **13**, 446–458 (2013).
11. Zhou, Z. *et al.* Brain-specific phosphorylation of MeCP2 regulates activity-dependent Bdnf transcription, dendritic growth, and spine maturation. *Neuron* **52**, 255–269 (2006).
12. Qi, L.S. *et al.* Repurposing CRISPR as an RNA-guided platform for sequence-specific control of gene expression. *Cell* **152**, 1173–1183 (2013).
13. Bikard, D. *et al.* Programmable repression and activation of bacterial gene expression using an engineered CRISPR-Cas system. *Nucleic Acids Res.* **41**, 7429–7437 (2013).
14. Gilbert, L.A. *et al.* CRISPR-mediated modular RNA-guided regulation of transcription in eukaryotes. *Cell* **154**, 442–451 (2013).
15. Grindberg, R.V. *et al.* RNA-sequencing from single nuclei. *Proc. Natl. Acad. Sci. USA* **110**, 19802–19807 (2013).
16. Moretti, P. *et al.* Learning and memory and synaptic plasticity are impaired in a mouse model of Rett syndrome. *J. Neurosci.* **26**, 319–327 (2006).
17. Kheirbek, M.A. *et al.* Differential control of learning and anxiety along the dorsoventral axis of the dentate gyrus. *Neuron* **77**, 955–968 (2013).
18. Chahrour, M. *et al.* MeCP2, a key contributor to neurological disease, activates and represses transcription. *Science* **320**, 1224–1229 (2008).
19. Hubel, D.H. & Wiesel, T.N. Receptive fields of single neurones in the cat's striate cortex. *J. Physiol. (Lond.)* **148**, 574–591 (1959).
20. Banerjee, A., Castro, J. & Sur, M. Rett syndrome: genes, synapses, circuits, and therapeutics. *Front. Psychiatry* **3**, 34 (2012).
21. Chao, H.T., Zoghbi, H.Y. & Rosenmund, C. MeCP2 controls excitatory synaptic strength by regulating glutamatergic synapse number. *Neuron* **56**, 58–65 (2007).
22. Wood, L., Gray, N.W., Zhou, Z., Greenberg, M.E. & Shepherd, G.M. Synaptic circuit abnormalities of motor-frontal layer 2/3 pyramidal neurons in an RNA interference model of methyl-CpG-binding protein 2 deficiency. *J. Neurosci.* **29**, 12440–12448 (2009).
23. McGraw, C.M., Samaco, R.C. & Zoghbi, H.Y. Adult neural function requires MeCP2. *Science* **333**, 186 (2011).
24. Feng, J. *et al.* Dnmt1 and Dnmt3a maintain DNA methylation and regulate synaptic function in adult forebrain neurons. *Nat. Neurosci.* **13**, 423–430 (2010).
25. Fu, Y. *et al.* High-frequency off-target mutagenesis induced by CRISPR-Cas nucleases in human cells. *Nat. Biotechnol.* **31**, 822–826 (2013).
26. Hsu, P.D. *et al.* DNA targeting specificity of RNA-guided Cas9 nucleases. *Nat. Biotechnol.* **31**, 827–832 (2013).
27. Cong, L. *et al.* Multiplex genome engineering using CRISPR/Cas systems. *Science* **339**, 819–823 (2013).
28. Fonfara, I. *et al.* Phylogeny of Cas9 determines functional exchangeability of dual-RNA and Cas9 among orthologous type II CRISPR-Cas systems. *Nucleic Acids Res.* **42**, 2577–2590 (2014).
29. Esvelt, K.M. *et al.* Orthogonal Cas9 proteins for RNA-guided gene regulation and editing. *Nat. Methods* **10**, 1116–1121 (2013).
30. Platt, R.J. *et al.* CRISPR-Cas9 knockin mice for genome editing and cancer modeling. *Cell* doi:10.1016/j.cell.2014.09.014 (24 September 2014).

ONLINE METHODS

Animals. The MIT Committee on Animal Care (CAC) approved all animal procedures described here. Adult (12-26 weeks old) male C57BL/6N mice were used in the study.

DNA constructs. For SpCas9 targets selection and generation of single guide RNA (sgRNA), the 20-nt target sequences were selected to precede a 5′-NGG protospacer-adjacent motif (PAM) sequence. To minimize off-targeting effects, the CRISPR design tool was used (http://crispr.mit.edu/). sgRNA was PCR amplified using U6 promoter as a template with forward primer: 5′-CGCACGCGTAATTCGAACGCTGACGTCATC-3′ and reverse primer containing the sgRNA with 20-nt DNA target site (**bold**): 5′-CACACGCGT AAAAAAGCACCGACTCGGTGCCACTTTTTCAAGTTGATAACGGACT AGCCTTATTTTAACTTGCTATTTCTAGCTCTAAAAC*NNNNNNNNNNN NNNNNNNNNC*GGTGTTTCGTCCTTTCCAC-3′. Control sgRNA sequence was designed to target *lacZ* gene from *Escherichia coli* (target sequence: TGCGAATACGCCCACGCGATGGG). EGFP-KASH[7] construct was a generous gift from Prof. Worman (Columbia University, NYC) and was used as PCR template for cloning the coding cassette into AAV backbone under the human *Synapsin* promoter (*hSyn*). U6-*Mecp2*sgRNA coding sequence was introduced using Mlu I site. For the multiplex gene targeting strategy, individual sgRNAs were PCR amplified as described above. All three sgRNAs were ligated with PCR amplified *hSyn*-GFP-KASH-bGHpA cassette (**Fig. 4a**) by using the Golden Gate cloning strategy. After PCR amplification, the ligation product containing three sgRNAs and *hSyn*-GFP-KASH-bGH pA was cloned into AAV backbone. All obtained constructs were sequenced verified. In order to find the optimal promoter sequence to drive SpCas9 expression in neurons we tested: hSyn1, mouse truncated *Mecp2* (pMecp2*)*, and truncated rat *Map1b* (pMap1b) promoter sequences[6] (**Supplementary Fig. 1a**). The following primers were used to amplify promoter regions: hSyn_F: 5′-GT GTCTAGACTGCAGAGGGCCCTG-3′; hSyn_R: 5′-GTGTCGTGCCTGAG AGCGCAGTCGAGAA-3′; Mecp2_F 5′-GAGAAGCTTAGCTGAATGGGG TCCGCCTC-3′; Mecp2_R 5′-CTCACCGGTGCGCGCAACCGATGCCGG GACC-3′; Map1b-283/-58_F 5′-GAGAAGCTTGGCGAAATGATTTGCTG CAGATG-3′; Map1b-283/-58_R 5′-CTCACCGGTGCGCGCGTCGCCTCC CCCTCCGC-3′.

Another truncation of rat *map1b* promoter was assembled with the following oligos: 5′-AGCTTCGCGCCGGGAGGAGGGGGGACGCAGTGGG CGGAGCGGAGACAGCACCTT CGGAGATAATCCTTTCTCCTGCCGCA GAGCAGAGGAGCGGCGGGAGAGGAACACTT CTCCCAGGCTTTAGC AGAGCCGGA-3′ and 5′-CCGGTCCGGCTCTGCTAAAGCCTGG GAGAA GTGTTCCTCTCCCGCCGCTCCTCTGCTCTGCGGCAGGAGAAAGGAT TATCTCCGAAGGTGCTGTCTCCGCTCCGCCCACTGCGTCCCCCCTC CTCCCGGCGCGA-3′. Short synthetic polyadenylation signal (spA)[31] was assembled using the following DNA oligonucleotides: 5′-AATTCAATAAAA GATCTTTATTTTCATTAGATCTGTGTGTTGGTTTTTTGTGTGC-3′ and 5′-GGCCGCACACAAAAAACCAACACACAGATCTAATGAAAATAAAG ATCTTTT ATTG-3′. SpCas9 and its D10A/H840A mutant version (dSpCas9) were described previously[27,32,33]. Plasmid encoding red fluorescent protein (mCherry) under control of EF1α promoter was used for neuron transfection with Lipofectamine 2000 (Life Technologies).

Cell line cultures and transfection. Neuro-2a (N2a) cells were grown in DMEM containing 5% FBS (BSA). For HEK293FT cells DMEM containing 10% FBS (FBS) was used. Cells were maintained at 37 °C in 5% CO_2 atmosphere. Cells were transfected using Lipofectamine 2000 or Polyethylenimine (PEI) "MAX" reagent (Polysciences), according to manufacturer's protocols.

Production of concentrated AAV vectors. High titer AAV1/2 particles were produced using AAV1 and AAV2 serotype plasmids at equal ratios and pDF6 helper plasmid in HEK293FT and purified on heparin affinity column[34]. Titering of viral particles was done with qPCR. High titer AAV1 particles were produced by the UNC Vector Core Services (University of North Carolina at Chapel Hill). Low titer AAV1 particles in DMEM were produced as described previously[35]. Briefly, HEK293FT cells were transfected with transgene plasmid, pAAV1 serotype plasmid and pDF6 helper plasmid using PEI "MAX". Culture medium was collected after 48 h and filtered through a 0.45 µm PVDF filter (Millipore).

Primary cortical neuron culture. Primary cultures were prepared from embryonic day 16 mouse brains[36]. Embryos of either sex were used. Cells were plated on poly-ᴅ-lysine (PDL)-coated 24-well plates (BD Biosciences) or laminin/PDL-coated coverslips (VWR). Cultures were grown at 37 °C and 5% CO_2 in Neurobasal medium, supplemented with B27, Glutamax (Life Technologies) and penicillin/streptomycin mix.

For AAV transduction, cortical neurons in 500 µl Neurobasal culture medium were incubated at 7 DIV with up to 300 µl (double infection at 1:1 ratio) AAV1-containing conditioned medium from HEK293FT cells[35]. One week after transduction neurons have been harvested for downstream processing or fixed in 4% paraformaldehyde for immunofluorescent stainings or morphology analysis.

For visualization of neuronal morphology, cells at DIV7 were transfected with EF1α-mCherry expression vector using Lipofectamine 2000 (Life Technologies) for 1 week as previously described[37]. For measurement of total dendrite length, all dendrites of individual neurons were traced using ImageJ software. Quantification of the number of primary dendrites, dendritic tips and the Sholl analysis[38] were performed on images acquired with fluorescent microscope at a 40× objective (Zeiss AxioCam Ax10 microscope, Axiocam MRm camera). For dendrites number, ends of all non-axonal protrusions longer than 10 µm were counted. For Sholl analysis, concentric circles with 5 µm step in diameter were automatically drawn around the cell body, and the number of dendrites crossing each circle was counted using ImageJ software with a Sholl plug-in.

Cell culture preparation and purification of cell nuclei. 7 days after viral delivery, cells were harvested in 200 µl ice-cold PBS and cell pellets were spun down at 2,000*g* for 10 min at 4 °C. Cell pellets were swelled on ice for 5 min in 1 ml lysis buffer (10 mM β-glycerophosphate (pH 7.0), 2 mM MgCl₂, 1 mM PMSF, 1 mM β-mercaptoethanol, 1% Tween-20). 1 ml ddH₂O was added and lysate was kept on ice for 5 min before cell lysates were homogenized with Dounce homogenizer (Sigma); 20 times with pestle A, followed by 10 times with pestle B. 2 ml equilibration buffer (120 mM β-glycerophosphate pH 7.0, 2 mM MgCl₂, 1 mM PMSF, 1 mM β-mercaptoethanol, 50% glycerol) was added and nuclei were centrifuged (1,000*g* for 10 min at 4 °C) using a sucrose gradient (lower: 500 mM sucrose, 2 mM MgCl₂, 25 mM KCl, 65 mM β-glycerophosphate pH 7.0, 20% glycerol, 1 mM PMSF, 1 mM β-mercaptoethanol; upper: 340 mM sucrose, 2 mM MgCl₂, 25 mM KCl, 65 mM β-glycerophosphate (pH 7.0), 20% glycerol, 1 mM PMSF, 1 mM β-mercaptoethanol). Number and quality of purified nuclei was controlled using bright-field microscopy.

Stereotactic injection of AAV1/2 into the mouse brain. Mice were anesthetized by intraperitoneal (i.p.) injection of 100 mg/kg ketamine and 10 mg/kg xylazine. Preemptive analgesia was given (Buprenex, 1 mg/kg, i.p.). Craniotomy was performed according to approved procedures, and 1 µl of 1:1 AAV mixture ($1 × 10^{13}$ vector genomes (Vg)/ml) of *sMecp2*-SpCas9; $6 × 10^{12}$ Vg/ml of DNMT 3×sgRNA; $3–5 × 10^{12}$ Vg/ml of h*Syn*-GFP-KASH) was injected into: dorsal dentate gyrus (anterior/posterior: −1.7; mediolateral: 0.6; dorsal/ventral: −2.15) and/or ventral dentate gyrus (anterior/posterior: −3.52; mediolateral: 2.65; dorsal/ventral: −3). For *in vivo* electrophysiology recording experiments (**Fig. 4**), virus injection coordinates were 3 mm lateral (from Bregma) and 1 mm anterior from the posterior suture. The skull was thinned using a dremel drill with occasional cooling with saline, and the remaining dura was punctured using a glass micropipette filled with the virus suspended in mineral oil. Several injections (3–4) were made at neighboring sites, at a depth of 200–250 µm. A volume of 150–200 nl of virus mixture was injected at 75 nl/min rate at each site. After each injection, the pipette was held in place for 3-5 min before retraction to prevent leakage. The incision was sutured and proper post-operative analgesics (Meloxicam, 1–2 mg/kg) were administered for 3 d following surgery.

***In vivo* two-photon guided targeted loose patch recordings.** Two weeks after virus injection, mice were used for electrophysiology experiments. Mice were anesthetized with 2% isoflurane and maintained using 0.8% isoflurane. The

skin was excised, cleaned with sugi and a metal head plate was attached to the skull using glue and dental acrylic, and a 2 × 2 mm craniotomy was performed over the primary visual cortex (V1). The exposed area was then covered with a thin layer of 1.5% agarose in artificial cerebrospinal fluid (aCSF; 140 mM NaCl, 5 mM KCl, 2 mM CaCl$_2$, 1 mM MgCl$_2$, 0.01 mM EDTA, 10 mM HEPES, 10 mM glucose; pH 7.4). Animal body temperature was maintained during experiment 37.5 °C with a heating blanket.

Borosilicate pipettes (WPI) were pulled using a Sutter P-2000 laser puller (Sutter Instruments). Tip diameter was around 1 μm while the resistance was between 3–5 MΩ. Recordings were made using custom software (Network Prism, Sur lab), written in Matlab (MathWorks), controlling a MultiClamp 700B amplifier (Axon). A glass pipette electrode was inserted into the brain at an angle of 20–35 degrees and an Ag/AgCl ground electrode pellet (Warner Instruments) was positioned in the same solution as the brain and the objective. For fluorescent visualization, pipettes were filled with Alexa Fluor 594 (Molecular Probes). The pipette was first targeted to the injection site using a 10× lens, and then targeted to individual GFP$^+$ cells using a 25× lens via simultaneous two-photon imaging at 770 nm. Cell proximity was detected through deflections in resistance observed in voltage clamp during a rapidly time-varying 5 mV command voltage pulse. Once resistance had increased by 5–10 MΩ, the amplifier was switched to current clamp, and spikes were recorded with zero injected current, under a Bessel filter of 4 KHz and an AC filter of 300 Hz. Virus-injected brains were perfused *post hoc* and immuno-histochemistry was performed.

Visual stimulation and data analysis from *in vivo* two-photon–guided targeted loose patch recordings. Oriented gratings using custom software written in Matlab PsychToolbox-3 were presented to assess the orientation selectivity and tuning of genome-edited neurons. Gratings were optimized for cellular responsiveness and were presented by stepping the orientation from 0–360 degrees in steps of 20 degrees, with each grating presentation being preceded for 4 s "off" followed by 4 s "on," for a total presentation duration of 144 s. Data were acquired directly into Matlab. Spike detection was performed via analysis routines that used manually defined thresholds followed by spike shape template matching for further verification. Every spike was tagged and displayed on screen in a graphical user interface whereupon it was manually reviewed for false positives and negatives by the experimenter. Spike times in response to every stimulus were then grouped into "on" or "off" periods based on their timing relative to visual stimulation, and "on" spikes for each stimulus were decremented by the number of "off" spikes observed during an equal time period. For orientation experiments, # spikes per stimulus = (# spikes "on") – (# spikes "off") because "on" and "off" periods were the same duration.

For every cell of interest, the methods were used to collect responses for each oriented stimulus (0 to 360 degrees, in steps of 20 degrees). These responses were then turned into a "tuning curve" of orientation versus response for each trial. Orientation Selectivity Index (OSI) was computed by taking the vector average for the preferred orientation:

$$OSI = \frac{\sqrt{\left(\sum_i R(\theta_i)\sin(2\theta_i)\right)^2 + \left(\sum_i R(\theta_i)\cos(2\theta_i)\right)^2}}{\sum_i R(\theta_i)}$$

Tissue preparation and purification of cell nuclei. Total hippocampus of adult male mice was quickly dissected in ice cold DPBS (Life Sciences). Dentate gyrus (DG) samples were prepared and separated from Ammon's horn (CA) as described elsewhere[39]. Samples were directly used for downstream analysis or shock frozen on dry ice. For cell nuclei purification, dissected tissue was gently homogenized in 2 ml ice-cold homogenization buffer (HB) (320 mM sucrose, 5 mM CaCl, 3 mM Mg(Ac)$_2$, 10 mM Tris pH7.8, 0.1 mM EDTA, 0.1% NP40, 0.1 mM PMSF, 1 mM β-mercaptoethanol) using 2 ml Dounce homogenizer (Sigma); 25 times with pestle A, followed by 25 times with pestle B. Next, 3 ml of HB was added up to 5 ml total and kept on ice for 5 min. For gradient centrifugation, 5 ml of 50% OptiPrep density gradient medium (Sigma) containing 5 mM CaCl, 3 mM Mg(Ac)$_2$, 10 mM Tris pH 7.8, 0.1 mM PMSF, 1 mM β-mercaptoethanol was added and mixed. The lysate was gently loaded on the top of 10 ml 29% iso-osmolar OptiPrep solution in a conical 30 ml centrifuge tube (Beckman Coulter, SW28 rotor). Samples were centrifuged at 10,100 × g (7,500 r.p.m.) for 30 min at 4 °C. The supernatant was removed and the nuclei

pellet was gently resuspended in 65 mM β-glycerophosphate (pH 7.0), 2 mM MgCl$_2$, 25 mM KCl, 340 mM sucrose and 5% glycerol. Number and quality of purified nuclei was controlled using bright-field microscopy.

Cell nuclei sorting. Purified KASH-GFP-positive (GFP$^+$) and negative (GFP$^-$) intact nuclei were co-labeled with Vybrant DyeCycle Ruby Stain (1:500, Life Technologies) and sorted using BD FACSAria III (Koch Institute Flow Cytometry Core, MIT). After sorting, all samples were kept on ice and centrifuged at 10,000g for 20 min at 4 °C. Nuclei pellets were stored at −80 °C or were directly used for downstream processing. Single-cell nuclei were sorted using Beckman Coulter MoFlo Astrios EQ Cell Sorter (FACS Center for Systems Biology, Harvard University) in 5 μl of QuickExtract DNA Extraction Kit (Epicentre) in 96-well format.

Genomic DNA extraction and SURVEYOR assay. For functional testing of sgRNA, 50–70% confluent N2a cells were co-transfected with a single PCR amplified sgRNA and SpCas9 vector. Cells transfected with SpCas9 only served as negative control. Cells were harvested 48 h after transfection, and DNA was extracted using DNeasy Blood & Tissue Kit (Qiagen) according to the manufacturer's protocol. To isolate genomic DNA from AAV1 transduced primary neurons, DNeasy Blood & Tissue Kit was used 7 d after AAV transduction, according to the manufacturer's instruction.

Sorted nuclei of dissected tissues were lysed in lysis buffer (10 mM Tris, pH 8.0, 10 mM NaCl, 10 mM EDTA, 0.5 mM SDS, 1 μg/μl of proteinase K and 50 ng/μl RNase A) at 55 °C for 30 min. Next, chloroform-phenol extraction was performed followed by DNA precipitation with ethanol, according to standard procedures. DNA was finally resuspended in TE Buffer (10 mM Tris pH 8.0, 0.1 mM EDTA) and used for downstream analysis. Functional testing of individual sgRNAs was performed with SURVEYOR nuclease assay (Transgenomics) using PCR primers listed in **Supplementary Table 2**. Band intensity quantification was performed as described before[40]. For next-generation sequencing, DNA of single-cell nuclei was extracted in QuickExtract DNA Extraction Kit (Epicentre) according to the manufacturer's protocol.

RNA library preparation and sequencing. Two weeks after bilateral viral delivery of SpCas9 with guide targeting *Mecp2* (four animals) or SpCas9 with gRNA targeting *lacZ* (four animals), DG and CA1 regions of hippocampus were quickly dissected in ice cold DPBS (Life Sciences) as previously described[39] and transferred immediately to RNA-later solution (Ambion). After 24 h in 4 °C the tissue was moved to −80 °C. Populations of 100 targeted neuronal nuclei were FACS sorted into 10 μl of TCL buffer supplemented with 1% 2-mercaptoethanol (Qiagen), centrifuged for 1 min and then frozen immediately on dry ice. RNA was purified by AMPure RNAcleanXP SPRI beads (Beckman Coulter Genomics) following the manufacturer's instructions, and washed three times with 80% ethanol, omitting the final elution. The beads with captured RNA were air-dried and processed immediately for cDNA synthesis. Samples with no nuclei were used as negative controls. Three DG population samples were used from each animal, to a total of 24 population samples, and an additional 6 population samples taken from the CA1 region of control animals. From each sample a cDNA library was prepared following the SMART-seq2 protocol as previously done[41], only replacing the reverse transcriptase enzyme with 0.1 μl of Maxima H Minus enzyme (200 U/μl, Thermo Scientific), and scaling down the PCR reaction to a volume of 25 μl. The tagmentation reaction and final PCR amplification were done using the Nextera XT DNA Sample preparation kit (Illumina), with the following modifications: all reaction volumes were scaled down by a factor of 4, and the libraries were pooled after the PCR amplification step by taking 2.5 μl of each sample. The pooled libraries were cleaned and size-selected using two rounds of 0.7 volume of AMPure XP SPRI bead cleanup (Beckman Coulter Genomics). Samples were loaded on a High-Sensitivity DNA chip (Agilent) to check the quality of the library, whereas quantification was done with Qubit High-Sensitivity DNA kit (Invitrogen). The pooled libraries were diluted to a final concentration of 4 nM and 12 pmol and were sequenced using the Illumina MiSeq Personal Sequencer (Life Technologies) with 75 bp paired end reads.

RNA libraries data analysis. Bowtie2 index was created based on the mouse mm9 UCSC genome and known Gene transcriptome[42], and paired-end reads

were aligned directly to this index using Bowtie2 with command line options -q–phred33-quals -n 2 -e 99999999 -l 25 -I 1 -X 1000 -a -m 200 –p 4–chunkmbs 512. Next, RSEM v1.27 was run with default parameters on the alignments created by Bowtie2 to estimate expression levels. The gene level expression estimates (tau) calculated by the RSEm program, were multiplied by 1,000,000 to obtain transcript per million (TPM) estimates for each gene, and TPM estimates were transformed to log-space by taking log(TPM+1). Genes were considered detected if their transformed expression level was equal to or above 1 (in log(TPM+1) scale). A library was filtered out if it had less than 8,000 genes detected. Based on this criterion, four libraries were filtered out and excluded from the downstream analysis. To test the specificity of the dissected brain regions, we chose known marker genes in the dentate gyrus region (*Igfbp5*, *Tdo2 and Dsp*) and in the CA1 region (*Nov*) and additional shared neuronal markers (*Gria1 and Camk2a*), and tested their relative expression levels (in log(TPM+1) units) within the DG samples and the CA1 samples in control animals (**Supplementary Fig. 8**). To find differentially expressed genes between control animals and Mecp2 sgRNA expressing animals, Student's *t*-test (Matlab V2013b) with correction for multiple hypothesis testing (Benjamini-Hochberg FDR procedure, $q < 0.01$) was performed. The *t*-test was run only on the highly expressed genes, which were defined to have mean expression level above 0.9 quantile (~6 log(TPM+1)) across all chosen samples. The expression levels (in log(TPM+1) units) of the differentially expressed genes across samples were clustered using hierarchical clustering (Matlab V2013b).

Immunofluorescent staining. For immunofluorescent staining of primary neurons, cells were fixed 7 d after viral delivery with 4% paraformaldehyde (PFA) for 20 min at room temperature (RT). After washing three times with PBS, cells were blocked with 5% normal goat serum (NGS) (Life Technologies), 5% donkey serum (DS) (Sigma) and 0.1% Triton X-100 (Sigma) in PBS for 30 min at RT. Cells were incubated with primary antibodies in 2.5% NGS, 2.5% DS and 0.1% Triton X-100 for 1 h at RT or overnight at 4 °C. After washing three times with PBST, cells were incubated with secondary antibodies for 1 h at RT. Finally, coverslips were mounted using VECTASHIELD HardSet Mounting Medium with DAPI (Vector Laboratories) and imaged using Zeiss AxioCam Ax10 microscope and an Axiocam MRm camera. Images were processed using the Zen 2012 software (Zeiss). Quantifications were performed by using ImageJ software 1.48 h and Neuron detector plugin.

Mice were euthanized 4 weeks after viral delivery by a lethal dose of ketamine/xylazine and transcardially perfused with PBS followed by 4% PFA. Fixed tissue was sectioned using vibratome (Leica, VT1000S). Next, 30 µm sections were boiled for 2 min in sodium citrate buffer (10 mM tri-sodium citrate dehydrate, 0.05% Tween-20, pH 6.0) and cooled down at RT for 20 min. Sections were blocked with 4% normal goat serum (NGS) in TBST (137 mM NaCl, 20 mM Tris pH 7.6, 0.2% Tween-20) for 1 h. Sections were incubated with primary antibodies diluted in TBST with 4% NGS overnight at 4 °C. After three washes in TBST, samples were incubated with secondary antibodies. After washing with TBST three times, sections were mounted using VECTASHIELD HardSet Mounting Medium with DAPI and visualized with confocal microscope (Zeiss LSM 710, Zen 2012 Software).

Following primary antibodies were used: rabbit anti-MeCP2 (07-013, Millipore, 1:200); mouse anti-NeuN (A60, Millipore, 1:50-1:400); chicken anti-GFAP (ab4674, Abcam, 1:400); mouse anti-Map2 (HM-2, Sigma, 1:500); chicken anti-GFP (1020, Aves labs, 1:200-1:400); rabbit anti-HA (C29F4, Cell Signaling, 1:100). Secondary antibodies: Alexa Fluor 488, 568 or 633 (Life Technologies, 1:500-1:1,000).

Quantification of LIVE/DEAD assay. Control and transduced primary neurons were stained using the LIVE/DEAD assay (Life Technologies) according to the manufacturer's instruction. To avoid interference with the GFP signal from GFP-KASH expression, cells were stained for DEAD (ethidium homodimer) and DAPI (all cells) only. Stained cells were imaged using fluorescence microscopy and DEAD, GFP- and DAPI-positive cells were counted by using ImageJ 1.48h software and Neuron detector plug-in.

Western blot analysis. Transduced primary cortical neurons (24-well, 7 d after viral delivery) or transduced tissue samples (4 weeks after viral delivery) were lysed in 50 µl of ice-cold RIPA buffer (Cell Signaling) containing 0.1% SDS and proteases inhibitors (Roche, Sigma). Cell lysates were sonicated for 5 min in a Bioruptor sonicater (Diagenode) and protein concentration was determined using the BCA Protein Assay Kit (Pierce Biotechnology, Inc.). Protein lysates were dissolved in SDS-PAGE sample buffer, separated under reducing conditions on 4–15% Tris-HCl gels (Bio-Rad) and analyzed by western blotting using primary antibodies: rabbit anti-Dnmt3a (H-295, Santa Cruz, 1:500), mouse anti-Dnmt1 (60B1220.1, Novus Biologicals, 1:800), rabbit anti-MeCP2 (07-013, Millipore, 1:400), mouse anti-HA (6E2, Cell Signaling, 1:400) rabbit anti-Tubulin (AA2, Sigma, 1:10,000) followed by secondary anti-mouse and anti-rabbit HRP antibodies (Sigma-Aldrich, 1:10,000). GAPDH was directly visualized with rabbit HRP coupled anti-GAPDH antibody (14C10, Cell Signaling, 1:10,000). Tubulin or GAPDH served as loading control. Blots were imaged with ChemiDoc MP system with ImageLab 4.1 software (Bio-Rad), and quantified using ImageJ software 1.48 h.

Fear conditioning. 12-week-old C57BL/6N male mice were stereotactically injected with SpCas9 and *Mecp2* or DNMT targeting sgRNA vectors into the dorsal or dorsal+ventral DG regions, respectively. Animals were habituated to the experimenter and the behavior room for 7 d. SpCas9/*lacZ* gRNA-injected littermates served as controls. At day 1, mouse cages were placed into an isolated anteroom to prevent mice from hearing auditory cues before and after testing. Individual mice were placed into the fear conditioning chamber (Med Associates Inc.) and a 12 min habituation period was performed. After habituation the mice were placed back to their home cages. The next day (training day), individual mice were placed into the chamber and were allowed to habituate for 4 min. After another 20 s (pre-tone) interval, the tone (auditory cue) at a level of 85 dB, 2.8 kHz was presented for 20 s followed by 18 s delay interval before the foot-shock was presented (0.5 mA, 2 s). After the foot-shock, 40 s interval (post-tone/shock) preceded a next identical trial starting with the 20 s pretone period. The training trial was repeated six times before the mice were placed back to their home cages. At day 3 (testing day), mice were first placed in the conditioning (training) context chamber for 3 min. Next, mice were placed in an altered context-conditioning chamber (flat floor versus grid, tetrameric versus heptameric chamber, vanillin scent), and the testing trial was repeated. Freezing behavior was recorded and analysis was performed blind off-line manually and confirmed with Noldus EthoVision XT software (Noldus Information Technology).

Open field, novel object recognition and elevated plus maze test. During the open field test, animals were placed in the square arena with opaque walls (40×40 cm, Stoelting) for 10 min while their behavior was recorded. The total distance moved, velocity and time spent in the center of arena were scored.

For the novel object recognition test animals were familiarized with the arena (40×40 cm, Stoelting) for 10 min, 24 h before the experiment. During training phase, 2 identical objects (black spheres) were placed in the corners of the arena. Animals were positioned in the arena facing opposite wall to the objects and left free to explore for 5 min while their behavior was scored and recorded. After the training phase animals were returned to home cages. After 2 h of delay phase, object recognition test was performed. Animals were placed in the arena where one of the familiar objects was swapped with a novel one (white cube). Location of the novel object was alternated between animals. Animals were scored and recorded for 3 min. Based on the interaction time with objects a discrimination ratio (preference for novel object) was calculated: total novel object interaction time/total interactions time with both objects.

For the elevated plus maze test mice were placed at the junction of the open and closed arms of the maze (Stoelting), facing the open arm opposite to the experimenter and left to explore the maze for 5 min. During that time animal was tracked and recorded. The total distance traveled in the open arms and time spent in open arms were measured automatically with Ethovision software (Noldus).

Next-generation sequencing (NGS) analysis and indel detection. To find potential off-targets for the DNMT family genes, the "CRISPR Design Tool" (http://crispr.mit.edu/) was used. Targeted cell nuclei from dentate gyrus were FACS sorted 10 weeks after viral delivery and genomic DNA was purified as described above. For each gene of interest, the genomic region flanking

the CRISPR target site was amplified by a fusion PCR method to attach the Illumina P5 adaptors as well as unique sample-specific barcodes to the target amplicons (for on- and off-target primers see **Supplementary Table 3**)[26]. Barcoded and purified DNA samples were quantified by Qubit 2.0 Fluorometer (Life Technologies) and pooled in an equimolar ratio. Sequencing libraries were then sequenced with the Illumina MiSeq Personal Sequencer (Life Technologies), with 300 bp reads length.

The MiSeq reads for pooled nuclei were analyzed as described previously[26]. Briefly, reads were filtered by Phred quality (Q score) and aligned using a Smith-Waterman algorithm to the genomic region 50 nucleotides upstream and downstream of the target site. Indels were estimated in the aligned region from 5 nucleotides upstream to 5 nucleotides downstream of the target site (a total of 30 bp). Negative controls for each sample were used to estimate the inclusion or exclusion of indels as putative cutting events. We computed a maximum-likelihood estimator (MLE) for the fraction of reads having target-regions with true-indels, using the per-target-region-per-read error rate from the data of the negative control sample. The MLE scores for each off-target are listed in **Supplementary Table 1**.

The MiSeq reads for single nuclei was analyzed slightly differently. First, samples with count of reads less than 100 were removed from analysis. Sequencing reads were aligned separately to primer sequence and 10 bp genomic sequence taken from 3′ downstream of the primer sequence using a Smith-Waterman algorithm. Reads were filtered out if there was any indel found within the alignment. Next, reads were trimmed from the 10 bp genomic sequence and aligned to the 23 bp guide sequence (target sequence + PAM sequencing). An alignment is considered as having an indel if an indel is found within ±6 bp around the expected Cas9 cut site. Indel pattern distribution was obtained by counting alignments containing different indel sequences separately. In order to model sequencing error, reads were aligned to another 23 bp genomic sequencing on 3′ downstream of the 10 bp genomic sequencing used in previous alignment, and distribution of alignments containing indels, denoted as indel types, was quantified. Sequencing reads containing indel was modeled as Bernoulli random variable and the parameter was fitted with a gamma distribution. For the following analysis, we chose the threshold for sequencing error rate at the false discovery rate of 2%. Sequencing reads from each single nuclei were filtered in order to remove possible doublet contaminations, whose ratio of second dominant indel type to the first dominant indel type and ratio of the third dominant indel type to the second dominant indel type both were found higher than the threshold for sequencing error. Next each single nuclei was classified as (i) wild-type, if the fraction of reads containing indels was lower than the sequencing error threshold, (ii) double allelic modified, if the fraction of reads containing no indel was lower than the sequencing error threshold, (iii) single allelic modified, if it did not fit to the two scenarios.

Statistical analysis. If not stated otherwise data were analyzed with GraphPad Prism 6.0 software (Graphpad Software). Groups were compared using an unpaired, two sided *t*-test. Normal distribution was assumed. Data are shown as mean with s.e.m.

31. Levitt, N., Briggs, D., Gil, A. & Proudfoot, N.J. Definition of an efficient synthetic poly(A) site. *Genes Dev.* **3**, 1019–1025 (1989).
32. Jinek, M. *et al.* A programmable dual-RNA-guided DNA endonuclease in adaptive bacterial immunity. *Science* **337**, 816–821 (2012).
33. Sapranauskas, R. *et al.* The *Streptococcus thermophilus* CRISPR/Cas system provides immunity in *Escherichia coli*. *Nucleic Acids Res.* **39**, 9275–9282 (2011).
34. McClure, C., Cole, K.L., Wulff, P., Klugmann, M. & Murray, A.J. Production and titering of recombinant adeno-associated viral vectors. *J. Vis. Exp.* **57**, e3348 (2011).
35. Konermann, S. *et al.* Optical control of mammalian endogenous transcription and epigenetic states. *Nature* **500**, 472–476 (2013).
36. Banker, G. & Goslin, K. Developments in neuronal cell culture. *Nature* **336**, 185–186 (1988).
37. Swiech, L. *et al.* CLIP-170 and IQGAP1 cooperatively regulate dendrite morphology. *J. Neurosci.* **31**, 4555–4568 (2011).
38. Sholl, D.A. Dendritic organization in the neurons of the visual and motor cortices of the cat. *J. Anat.* **87**, 387–406 (1953).
39. Hagihara, H., Toyama, K., Yamasaki, N. & Miyakawa, T. Dissection of hippocampal dentate gyrus from adult mouse. *J. Vis. Exp.* **33**, 1543 (2009).
40. Ran, F.A. *et al.* Genome engineering using the CRISPR-Cas9 system. *Nat. Protoc.* **8**, 2281–2308 (2013).
41. Picelli, S. *et al.* Smart-seq2 for sensitive full-length transcriptome profiling in single cells. *Nat. Methods* **10**, 1096–1098 (2013).
42. Fujita, P.A. *et al.* The UCSC Genome Browser database: update 2011. *Nucleic Acids Res.* **39**, D876–D882 (2011).